ISSN 1070-4272, Russian Journal of Applied Chemistry, 2019, Vol. 92, No. 9, pp. 1291−1305. © Pleiades Publishing, Ltd., 2019.

ORGANIC SYNTHESIS
AND INDUSTRIAL ORGANIC CHEMISTRY

A Deep Analytical Study in the Oxidation Polymerization Desulfurization Process Using a Keggin-Type Polyoxometalate Catalyst: Characterization of Solid and Liquid Products

Seyed Hossein Mansourian[a], Shahrokh Shahhosseini[a,*], and Ali Maleki[b]

[a] *School of Chemical Engineering, Iran University of Science and Technology, Narmak, Tehran, 16846 Iran*
[b] *Catalysts and Organic Synthesis Research Laboratory, Iran University of Science and Technology, Tehran, 16846-13114 Iran*
**e-mail: Shahrokh@iust.ac.ir*

Received February 6, 2019; Revised July 6, 2019; Accepted July 10, 2019

Abstract—In this study, oxidation of a model fuel, benzothiophene (BT) in *n*-decane, using polyoxometalate catalyst with Keggin structure has been investigated. The solid product evaluation was performed using gel permeation chromatography (GPC), thermal gravimetric analysis (TGA)/(DSC) differential scanning calorimeter, FTIR, proton and carbon nuclear magnetic resonance ($^{1}H + {}^{13}C$ NMR) spectrums, elementary (C, H, N and S) analyses. The results showed that the solid product was a polymer with a weighted average molecular weight (Mw) of 183030. In addition, the polymer was found to be sticky, branched and cross-linked. Moreover, for the first time, the role of the different solvents in the formation of the polymer was studied. It was revealed that the solvent intermolecular force plays an important role in polymerization so that the solvent with stronger molecular force did not participant in the polymerization. Ultimately gas chromatography–flame ionization detector (GC-FID) analysis showed the amount of desulfurization was about 81%.

Keywords: oxidative desulfurization polymerization (OPD), polyoxometalate catalyst, cross-linked and network structure, benzothiophene (BT)

DOI: 10.1134/S1070427219090155

INTRODUCTION

In recent decades, fossil fuel consumption has increased and consequently emission rate of the pollutants such as sulfur has also soared, leading to one of the most challenging environmental and human health problems [1, 2]. Therefore, in most countries in the world, laws and regulations have been introduced to reduce sulfur content of the fuels such as gasoil and diesel [3–5]. The traditional gasoil desulfurization technology, hydro-ы desulfurization (HDS), involves high consumption of hydrogen and is operated at high pressure and temperature [6, 7]. In addition, HDS is not suitable to eliminate refractory aromatic sulfur compounds of gasoil, especially thiophene family (such as benzothiophene (BT) and dibenzothiophene (DBT)). Therefore new methods are to be developed to replace or to complement HDS [8–12].

Among the new methods, oxidative desulfurization (ODS) has received more attention from the researchers since this method can be applied under a temperature of less than 100°C and at atmospheric pressure [13–16]. This method employs a strong oxidative catalyst such as organic acids or polyoxometalates [17–20]. Polyoxometalates have many unique properties including their well-defined structures, the ability to accept and lose electrons, high oxidation potential, high thermal resistance, creating ideal conditions for the polymerization process of some monomers, and high flexibility of the structural modification [21–26]. Shojaei et al. [27], showed that the Keggin structure was more suitable for oxidation of the organic substrates than other structures of the polyoxometalates [18, 27]. The great attention paid to this structure is due to its high acidity and its oxidative potential, which is due to super activity and high proton mobility. These

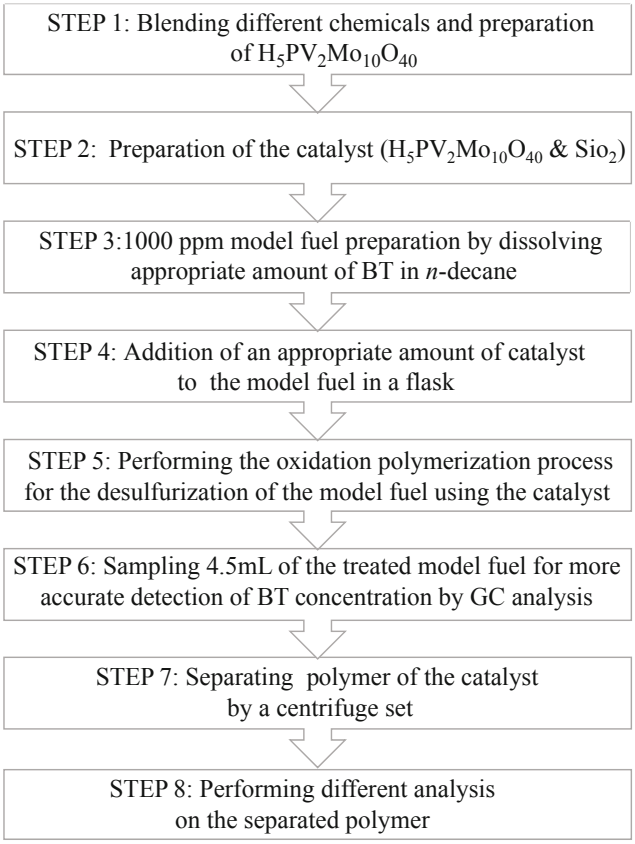

Fig. 1. An overview of all the laboratory steps for the desulfurization of BT model fuel by oxidation polymerization process.

characteristics are due to the existence of two vanadium atoms and ten molybdenum atoms, leading to increase potential reduction to 0.7 (SHE – 0.7) [18, 28, 29]. In addition, due to the difficulty of separating the catalyst in the homogeneous state, the researchers preferred to use this catalyst that is heterogeneous [17, 30, 31]. For instant, Zhu et al. [30], in 2013 used polyoxometalate catalyst with hydrogen peroxide and succeeded in desulfurization (98.4%) of a model fuel containing DBT. In the same year, Xiao et al. [32], used the tungsten compound of the polyoxometalate family for desulfurization of a model fuel containing BT (88.2%). Li et al. [33], also used silica-amino (SBA15) and molybdovanadophosphoric acid with hydrogen peroxide, which resulted in more than 98% sulfur removal of a DBT containing fuel. Yan et al. [34], used a binary combination of silica-titania for polyoxometalate catalyst with hydrogen peroxide that could remove more than 98% sulfur content of a DBT containing model fuel. In 2016, Choi et al. [35], could achieve more than 97% desulfurization, using this catalyst, hydrogen peroxide and ultrasonic waves.

Studies showed that the use of hydrogen peroxide or the combination of polyoxometalate catalyst with organic or inorganic materials created the challenge of separating them from the catalyst and caused the process to be economically or environmentally unviable [36]. Neumann et al. succeeded in desulfurization of the model fuel, containing BT and DBT, using the Keggin structure of the polyoxometalate catalyst without any additional material [36]. Their results indicate that oxidative polymerization desulfurization (OPD) method could be used for desulfurization of a model fuel containing BT or DBT. In other word, OPD process is a method of separating BT and DBT from a fuel by converting these monomers into a polymer. However, they have not characterized the products obtained at the end of the desulfurization procedure, which means further investigations are required on this subject. Therefore, in this work, oxidative polymerization desulfurization process has been studied with more details, examining the characteristics of the produced polymer. In addition, the effect of the solvent of the model fuel on the polymerization process has been investigated, for which three different solvents have been used.

EXPERIMENTAL

Chemicals

The chemicals used in this study such as BT (98.0%, BT), *n*-decane (94.0%), tetrahydrofuran (99.0%, THF), acetonitrile (99.0%), sulfuric acid (95–97%), diethyl ether (98.0%), silica gel 60 (10 g, Merck, 0.040–0.063 mm, surface area 480–540 $m^2 g^{-1}$), sodium metavanadate, Na_2HPO_4, $Na_2MoO_4 \cdot 2H_2O$ were prepared from Merck Co. (Germany). All of the listed chemicals were of analytical grades and were used without more purification.

Catalyst Synthesis and Characterization Methods

Figure 1 shows an overview of all the laboratory steps performed in a step-by-step and accurate procedure for the desulfurization of BT model fuel using oxidation polymerization process.

Preparation of $H_5PV_2Mo_{10}O_{40}$. Figure 2 shows the catalyst preparation steps as well as the desulfurization reactor. In step 1 of this figure $H_5PV_2Mo_{10}O_{40}$ is shown, which is obtained by combining the following materials. Sodium metavanadate (12.2 g, 100 mmol) was dissolved by boiling it in 50 mL of water and then mixing it with (3.55 g, 25 mmol) of Na_2HP0_4. After the solution was cooled to ambient temperature, concentrated sulphuric

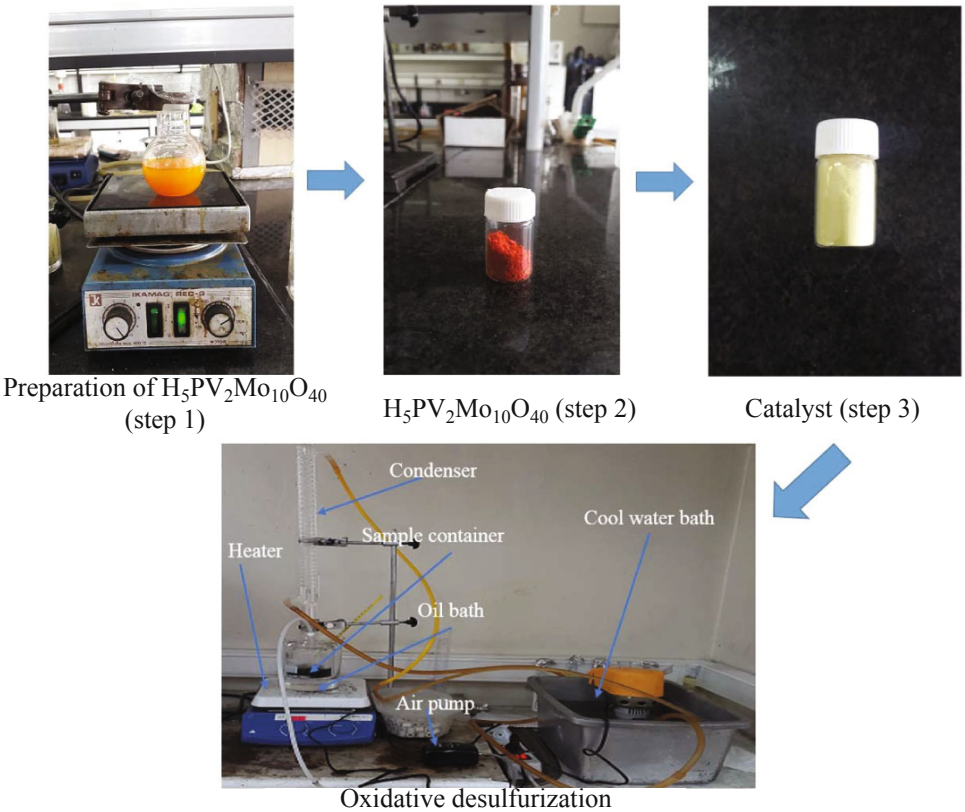

Fig. 2. (Color online) Catalyst preparation steps and the desulfurization process.

acid (5 mL, 17 M, 85 mmol) was added, where through a red color was developed. Then, $Na_2MoO_4{\cdot}_2H_2O$ (60.5 g, 250 mmol), dissolved in 100 mL of water, was added to the red solution obtained in the previous stage. In this step, the mixture was severely shaken for a specific time. During vigorous mixing, the concentrated sulphuric acid (42 mL, 17 M, 714 mmol) was slowly added with a dropper. The hot mixture was given time to cool down to the room temperature. The 10-molybdo-2-vanadophosphoric acid was then extracted with 500 mL of diethyl ether. Air was transferred through the heteropoly etherate (bottom layer) to free it of ether. The solid residue was dissolved in water, concentrated to first crystal formation, as already described, and then allowed to crystallize further. Finally as shown in step 2 of Fig. 2 the solid polyoxometalate catalyst was obtained by filtering the large red crystals, then washing it with water and drying it with air [24, 27, 36].

Preparation of $H_5PV_2Mo_{10}O_{40}/SiO_2$ catalyst. The wet impregnation method was used to prepare the catalyst as shown in step 3 of Fig. 2 by applying the following procedure. The red crystals obtained in the previous section ($H_5PV_2Mo_{10}O_{40}$ (1 g)) was dissolved in deionized water (50 mL). Then the silica gel powder (with the specifications that are, 10 g, Merck, 0.040–0.063 mm, surface area 480–540 $m^2\,g^{-1}$) suspended in deionized water (50 mL) was added to the mixture. The resulting mixture was stirred at room temperature for 6 h and the water was then evaporated under vacuum at specific time. $H_5PV_2Mo_{10}O_{40}/SiO_2$ was dried under reduced pressure for 4 h [36].

Phosphovanadomolybdate and the catalyst, prepared according to FTIR and EDX analysis, have been studied and characterized as follows: FTIR spectra were determined on a BrukerVector-22 infrared spectrometer using KBr disks. The number of scans was 32 and the resolution was 4 cm^{-1}. All spectra were collected in the range of 400–4000 cm^{-1}. In addition, the chemical composition of the sample was determined by EDX.

General Procedures for Oxidative Desulfurization Process

The model fuel was prepared by dissolving BT in *n*-decane, with a corresponding S-content of 1000 ppmw. As shown in step 4 of Fig. 2, in order to run the oxidative

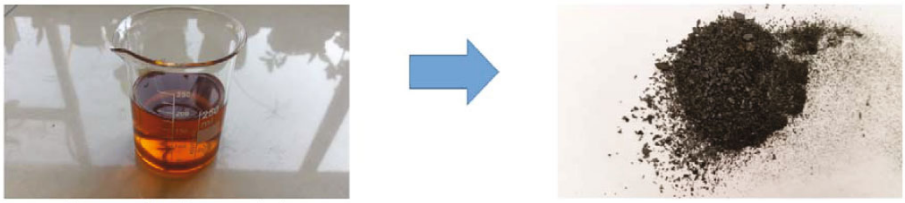

Separated polymer solution (including solvent and polymer) from the catalyst (step 1)

Polymer obtained after complete solvent evaporation (step 2)

Fig. 3. (Color online) A view of the procedure for separation of the polymer from the catalyst and the preparation of formed polymer.

desulfurization tests, 100 mg of the prepared catalyst (containing 9.1% $H_5PV_2Mo_{10}O_{40}/SiO_2$) and the model fuel were placed into a 50 mL reactor equipped with an air pump and a reflux condenser, on a heater, and stirred (with a magnetic stirring speed of 1000 rpm) at certain temperature for a determined time. In order to control the temperature, an oil bath was used on the heater and then the flask was placed inside the oil bath. After the reaction was completed, the mixture was cooled down to the room temperature and the upper clear solution was withdrawn to determine its sulfur conversion. In addition, at the end of the experiment, the remaining solid at the bottom of the flask was separated to analysis the produced polymer. The sulfur conversion (BT conversion) can be calculated as the difference between the amount of sulfur before entering the reactor and after exiting the reactor. In order to study, the typical sample characterized by GC-FID analyses were performed. Gas chromatographic analysis was conducted using Shimadzu GC-2010 (Kyoto, Japan) equipped with a split/split less injection port and a flame ionization detector (FID). The GC capillary column with an internal diameter of 0.25 mm which were coated with a 0.22 μm thick film of BP5 (5% phenyl siloxane, 95% methyl polyorganosiloxane; Supelco, Bellefonte, USA) was used. At the first step, six samples of the model fuel as index (with concentrations including (a) 1100, (b) 800, (c) 500, (d) 200, (f) 100, and (g) 50 ppm) were prepared and along with the obtained result after desulfurization, were analyzed.

General Procedure for Separation of the Polymer from the Catalyst

Figure 3 shows the steps taken to separate the polymer from the catalyst. In order to produce a detectable amount of polymer a model fuel with sulphur content of 20 000 ppm was used. 0.5 g of the catalyst was added to the fuel and the reaction was carried out. At the end of the reaction, the solid, composed of the catalyst and the polymer (the polymer was stuck on the catalyst) was precipitated at the bottom of the flask. Then the remaining solvent was removed. In the next step, a new solvent tetrahydrofuran (THF) was added to the flask to solve the polymer. Then, the new solution including the solvent, the polymer and the catalyst were poured into a number of falcons (15cc). The falcons were centrifuged at 8 000 rpm for 60 min leading to deposition of the catalyst at the bottom of the falcons. The supernatant of the falcons was gathered in a beaker as shown in step 2 of Fig. 3, which includes only THF and the polymer.

The remaining catalyst at the bottom of the falcons was weighted to be 0.5 g. The liquid in the beaker was allowed to evaporate for a few days tile all the solvent was evaporated so that only the dry polymer powder remained in the beaker. Step 2 of Fig. 3 shows the dark brown polymer powder. It should be noted that during the preparation of the polymer, its sticky physical state was observed.

In addition to the FTIR analysis, the analysis described below are used to identify and evaluate the polymer. Elementary (C, H, N, and S) analysis were performed with CHN–O–Rapid (Leeco Corporation – TruSpec model). Differential scanning calorimetry (DSC) measurement was performed on a METTLER TOLEDO instrument Switzerland) DSC1 Model, interfaced to a digital computer equipped with Star E 9.01 software (Sencor FRS5) and type of (Sample & reference) Pan: Aluminum Crucible Standard 40 μL. The samples were heated from 100 to +340°C with a rate of 10°C min^{-1}. The thermal gravimetric analysis of the polymer was determined by TGA/DSC (model DSC1). The sample (10–20 mg) was heated at the temperature range of 50–600°C under N_2 under and atmosphere. H + CNMR spectrums were recorded on an AV-400 spectrometer (Bruker Corporation,

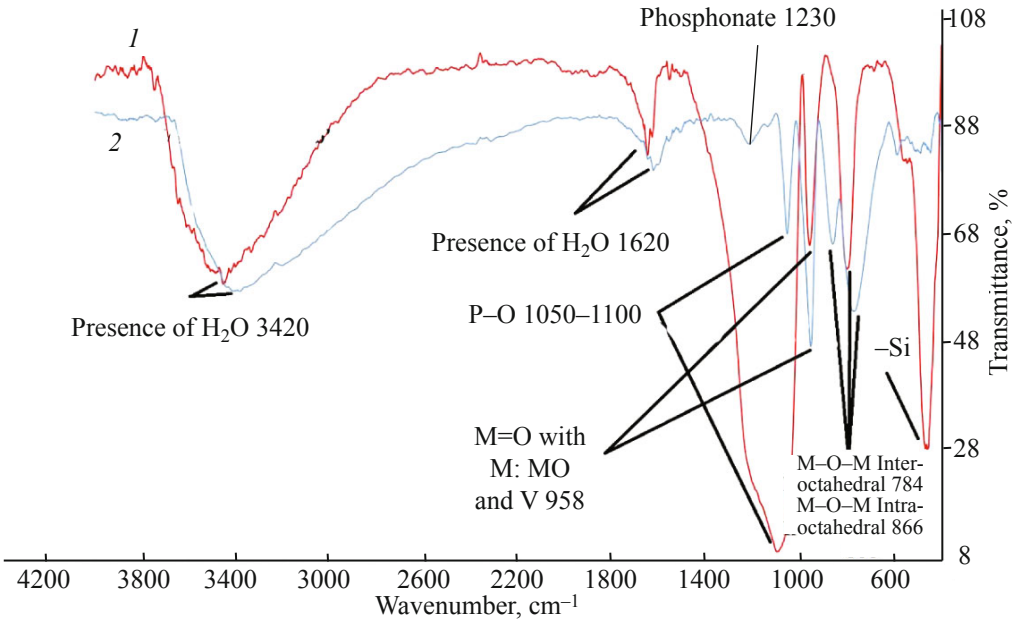

Fig. 4. (Color online) FTIR spectra of $H_5PV_2Mo_{10}O_{40}$ (*1*) polyoxometalate and (*2*) the silica-supported catalyst.

Germany) and a content of the samples (0.4–0.5 mg) is dissolved in (0.5–0.7 mL) DMSO. Molecular weight distribution and molecular weight averages were determined by gel chromatography (GPC) (model Yl9100, YL Instrument Corporation, Korean) at 135°C in THF running with a flow rate of 1.0 mL min^{-1}. The GPC was equipped with an automatic injection system, a dual-headed pump (model 9110) and a refractive index detector (model 9170). A set of four columns include styragel columns HT2, HT3, HT4, and HT5 include effective molecular weight ranges (100–10 k, 500–30 k, 5–600 k, and 50–4000 k) was used. Polystyrene standards were used for the calibration. Analysis was carried out in THF running with a flow rate of 1.0 mL min^{-1} at 35°C. Polystyrene standards were used for the calibration.

RESULTS AND DISCUSSION

The results are divided into three sections. (1) Catalyst preparation and characterization; (2) Desulfurization; (3) Characterization of the prepared polymer.

Step 1: The Characterization of the Keggin-Type Catalysts

Figure 4 shows the FTIR spectra of polyoxometalate ($H_5PV_2Mo_{10}O_{40}$) and the silica-supported catalyst. There are four characteristics infrared bands of the Keggin structure including 1057 cm^{-1} (ν_{as} P–O), 958 cm^{-1} (ν_{as} M=O, with M: Mo and V), 866 cm^{-1} (ν_{as} M–O–M inter-octahedral), 784 cm^{-1} (ν_{as} M–O–M intra-octahedral) in accordance with the literature [37, 38]. The band located at 1230 cm^{-1} presents a band of phosphonate (ν_{as} P=O). In addition, the bands placed at 3300–3500 cm^{-1} and 1610–1650 cm^{-1} confirms the presence of water in the structure (secondary structure). The variation of these vibrations toward lower wavenumbers for V-POM (i.e., 4–5 cm^{-1}) belongs to the reduced structure symmetry and confirms the presence of V-atom in the Keggin unit [38].

To ensure the existence of two vanadium atoms in the structure of the catalyst, an EDX elemental analysis was provided based on the work of Tsigdinos and Hallada [37–39]. This analysis presented further evidence for formation of Keggin structure containing the appropriate number of vanadium atoms. Figures. 5a and 5b show the results of the EDX of POM and silica-supported POM, respectively. As can be seen in Fig 5, the chemical composition of the typical sample is; silicon, molybdenum, phosphorus, oxygen and vanadium. Then, according to Table 1, the molar ratio of the elements in the Keggin structure ($H_5PV_2Mo_{10}O_{40}$), based on software calculation of the EDX analysis, are shown.

Table 1 shows molar ratios of the chemical elements of a typical $H_5PV_2Mo_{10}O_{40}$ sample, obtain using EDX analysis. Column (a) of this table gives the ratios obtained

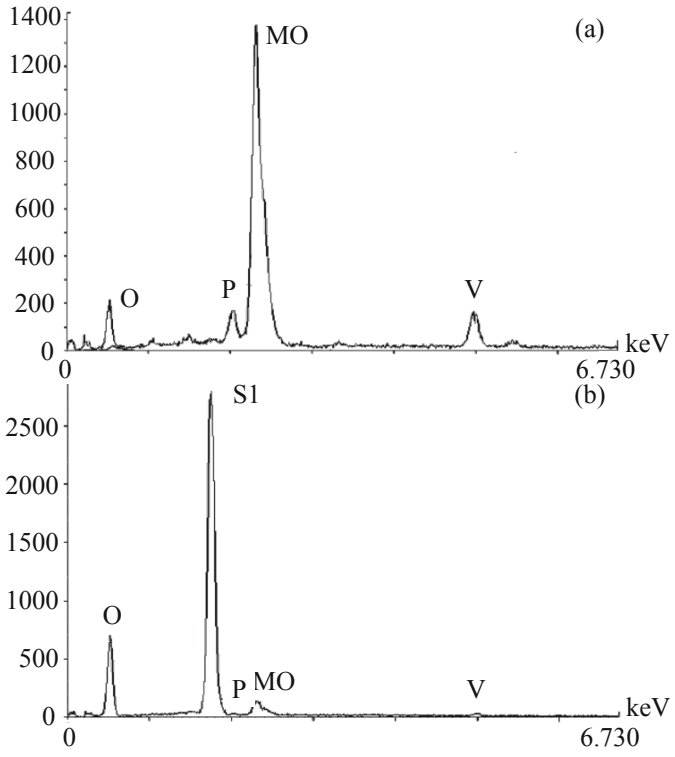

Fig. 5. EDX pattern of (a) $H_5PV_2Mo_{10}O_{40}$ and (b) $H_5PV_2Mo_{10}O_{40}/SiO_2$ (catalyst).

in this work and column (b) gives the ratios reported by Tsigdinos and Hallada [39]. These results indicate that the molar ratios of this work are very close to those of the literature.

Table 1. Molar ratios of chemical elements of a typical $H_5PV_2Mo_{10}O_{40}$ sample

Chemical element in $H_5PV_2Mo_{10}O_{40}$	Molar ratios (a)	Literature results (b) [39]
P	1.32	1.31
V	4.23	4.32
Mo	40.19	40.69
H and O	54.25	26.33

Step 2: Oxidative Desulfurization Rate of BT in the Presence of the Catalysts

In order to study the catalyst performance, ODS process was performed on a typical model fuel under the mentioned experimental condition. GC–FID analysis was used to determine the exact amount of oxidative desulfurization. Figure 6 shows the results obtained from the GC-FID analysis. In this regard, six samples of the model fuel as indexed with concentrations of (a) 1100, (b) 800, (c) 500, (d) 200, (f) 100, and (g) 50 ppm along with tested sample (e) were analyzed. As can be seen in Fig. 6, the appeared peaks are in descending process and area of the dropping peaks.

In Fig. 7, the areas of the peaks are plotted against the sample concentrations. Equation (1) was then fitted into the data of Fig. 7.

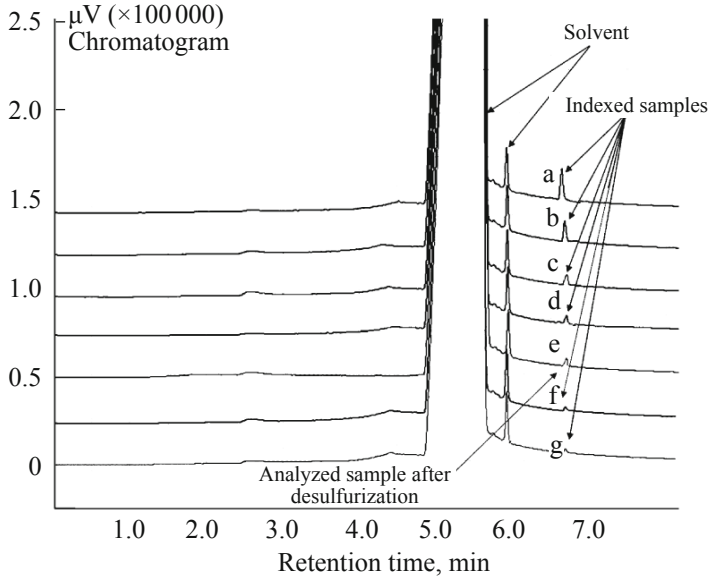

Fig. 6. GC-FID chromatograms of model fuels indicators before oxidation, ppm: (a) 1100, (b) 800, (c) 500, (d) 200, (f) 100, (g) 50 ppm, and after oxidation of model fuel (oxidative desulfurization sample (e), oxidation conditions: time 12 h, reaction temperature 75°C).

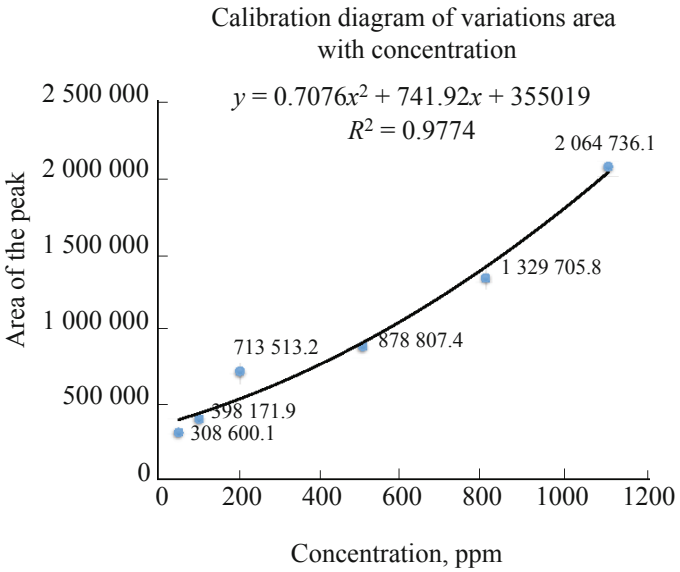

Fig. 7. The calibration diagram of the chromatogram analysis data (area of the peak and concentration of samples) and the equation fitted from data.

$$y = 0.7.907x^2 + 741.92x + 355019, \quad (1)$$

where y is area and x is concentration

Equation (2) can be used to calculate the desulfurization rate (80.15%) [15, 35].

$$S_t\,(\%) = \frac{S_{initial} - S_{final}}{S_{initial}} \times 100, \quad (2)$$

where $S_{initial}$ (1000 ppm) is the initial sulfur concentration in the model fuel and S_{final} (198.5 ppm) denotes the final sulfur concentration of model fuel, after oxidation reaction.

Step 3: The Characterization of the Polymeric Product from the Oxidative Polymerization Process

Before characterizing the polymer product, it is necessary to explain how the process the polymer is formed. Figure 8 shows the overall view along with the details of the polymerization process. Due to the existence of an empty d orbital in the vanadium atom in the catalyst structure, it strongly requires an electron capture. Thus, by attacking the structure of BT in the model fuel, it absorbs electron and converts them into a BT radical. As shown in reaction (I) of Fig. 8, the electron is transferred from BT to the catalyst, which reduces the catalyst and converts BT to a positive radical. This reaction is the first reaction (initiation of the polymerization process) and is shown as reaction (I) of Fig.8.

In the next step, the positive radicals of BT formed in reaction (I) have an electrophilic property that can

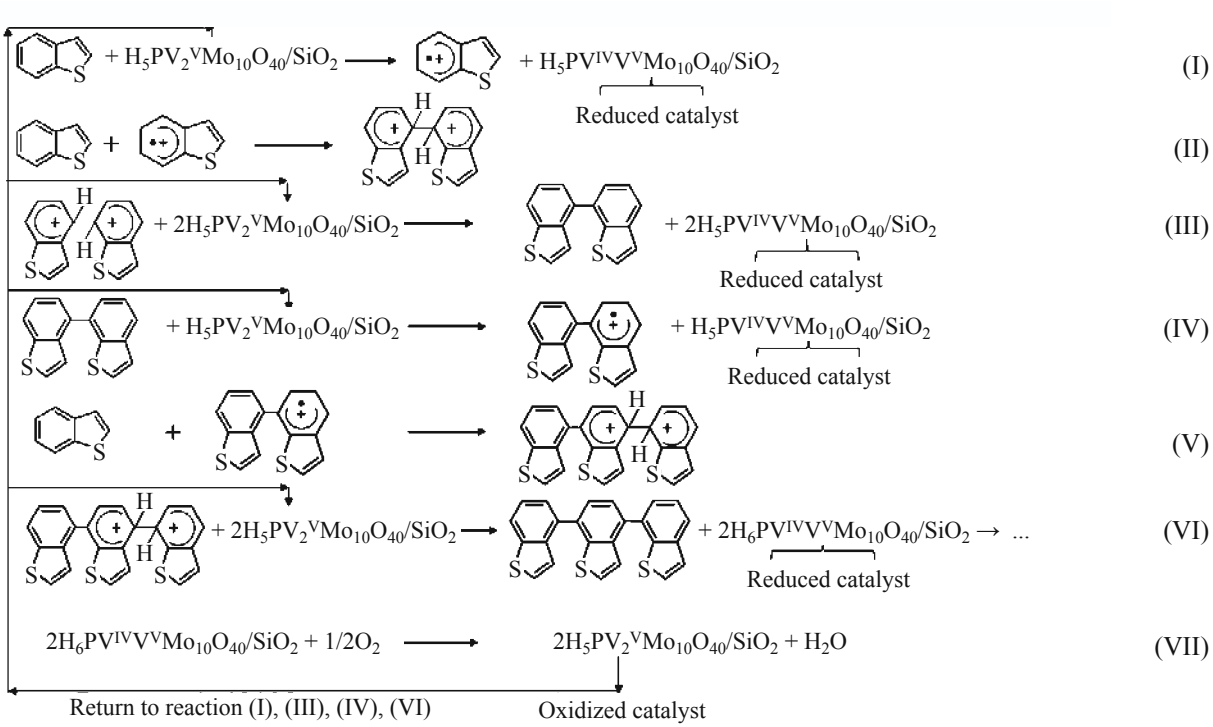

Fig. 8. A scheme of the oxidative polymerization desulfurization of the model fuel containing BT.

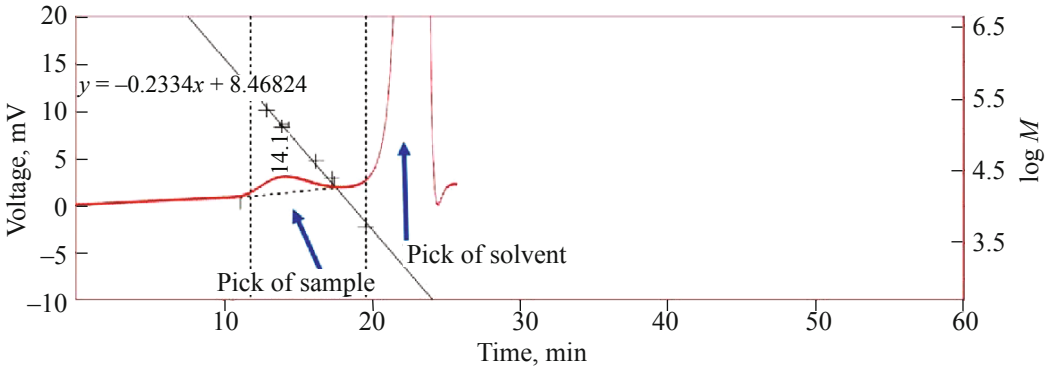

Fig. 9. (Color online) GPC curves of the polymer and solvent.

start an electrophilic aromatic substitution reaction in the presence of the other BT molecules. As shown in reaction (II) of Fig. 8, there is a binary radical of BT that it occurs by the electron donating property in an outer-sphere electron transfer mechanism [36, 40–42]. In reaction (III), the product of reaction (II) is re-attacked by the catalyst causing it to lose two electrons and become a dimmer of BT. The dimer obtained in reaction (III) converts to a trimmer through reactions (IV) to (VI). This process continues until all BT molecules or a part of BT molecules are converted into the polymer. According to reaction (VII), oxygen molecules, which are penetrated into the fuel from the ambient air, oxidize the catalyst and regenerate it. The catalyst capacity and the catalyst regeneration rate by oxygen are the main parameters, which determine how many of BT molecules can be converted into the polymer.

Table 2 Molecular weight distribution of typical sample by GPC analysis

MW distribution	M_n: 111911 Da
	M_w: 183030 Da
	M_p: 152446 Da
	M_z: 275336 Da
	M_{z1}: 367949 Da
	M_v: 171654 Da
	M_w/M_v: 1.06
	M_z/M_w: 1.50
	PDI= M_w/M_n: 1.63
	MWD = M_w/M_p: 1.2
Retention time, min	Start: 11.09
	Max: 14.07
	End: 17.43
	Sample Dilution: 1.00
	Unretained Peak Time: 0.00
Column Length: 0.05 Injection Volume: 0.025 Height (mV): 1.9 Area (Mv.s): 376.01	

After the oxidative polymerization process, a brown colored substance is deposited on the surface of the polyoxometalate catalyst. As Domb and Langer [43], have reported the acidic catalysts include intermediate metals such as titanium that can change the polymer color. After the separation of the brown precipitate from the catalyst, it was identified by conventional analytical techniques.

GPC analysis. Molecular weight (MW) of a polymer plays an important role in its synthesis and application. One of the most accurate methods for determining MW of a polymer is GPC analysis. To assure the formation of any polymer beside the present catalyst, GPC analysis was used to obtain the MW of the prepared polymer. The results obtained from GPC analysis is shown in Table 2 and Fig. 9. GPC curve is shown in Fig. 9. As it is observed from Fig. 9, there are two peaks for the solvent and a typical sample. The polymer formation can be confirmed by observing peak of the typical sample. In Table 2, MW distribution obtained from a sample of 0.05 g is shown in GPC analysis. As shown in Table 2, MW distribution well represent the polymer formation. Therefore, the numerical average MW (M_n = 111911 Da) and the weighted average MW (M_w = 183030 Da) confirm the polymer formation and also shows that the polymer has a narrow molecular

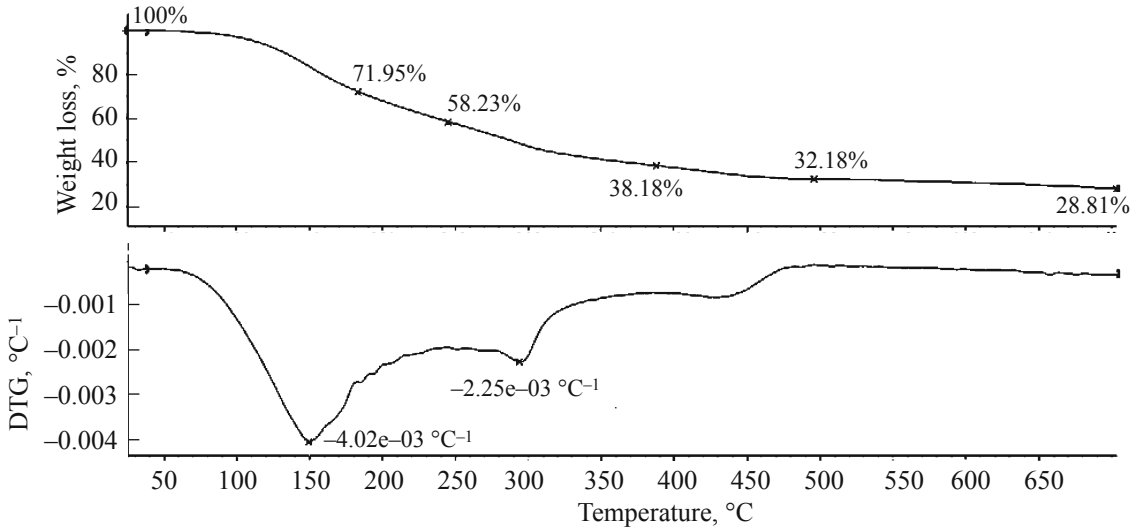

Fig. 10. TGA analysis of the prepared polymer.

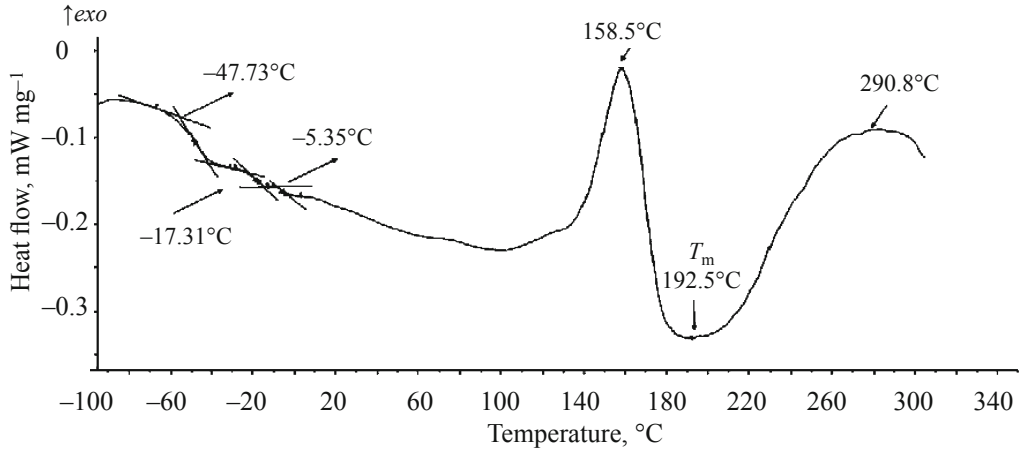

Fig. 11. DSC analysis of the prepared polymer.

weight distribution [44]. The definition of the average MW shown in Table 2 is presented in the literature by Shortt [45]. In addition, the polydispersity index (PDI = 1.635) is greater than 1 that indicates it is a polydisperse polymer [46]. The GPC data in Table 2 indicate that the polymerization has taken place.

Thermal analysis. TGA and DSC analyses were performed to study the thermal properties of the polymer. TGA is a simple and accurate method to see the decomposition pattern and the thermal stability a polymer by determining the weight loss of the polymer as a function of time or temperature. DSC is the best way to determine the glass transition temperature (T_g), and crystalline melting temperature (T_m) [44, 47]. In Figs. 10 and 11, the data obtained from TGA and DSC analyses are displayed.

Figure 10 indicates five different signal values. The main decomposition of the prepared polymer starts above 150 °C. Then, due to the destruction of C–C, C–S or S–S bonds it goes up to 650°C. At the end of the heating TGA analysis indicates that a significant amount of polymer (about 30%) remains at 650°C. It represents the ash content that can be due to aromatic compounds.

In addition, DSC test (data is in Fig. 11) was carried out on the sample at a heating rate of 10°C min^{-1}. In Figure 11, there are three different temperatures at –47.73, –17.31, and –5.35 °C that can be caused by T_β, T_α and T_g transition temperatures. The reason for having this glass transition temperatures can be stated according to the literature [48–50]. The reasons for observing these temperatures are the factors such as rotation of the functional groups, rotation and movement of the parts of

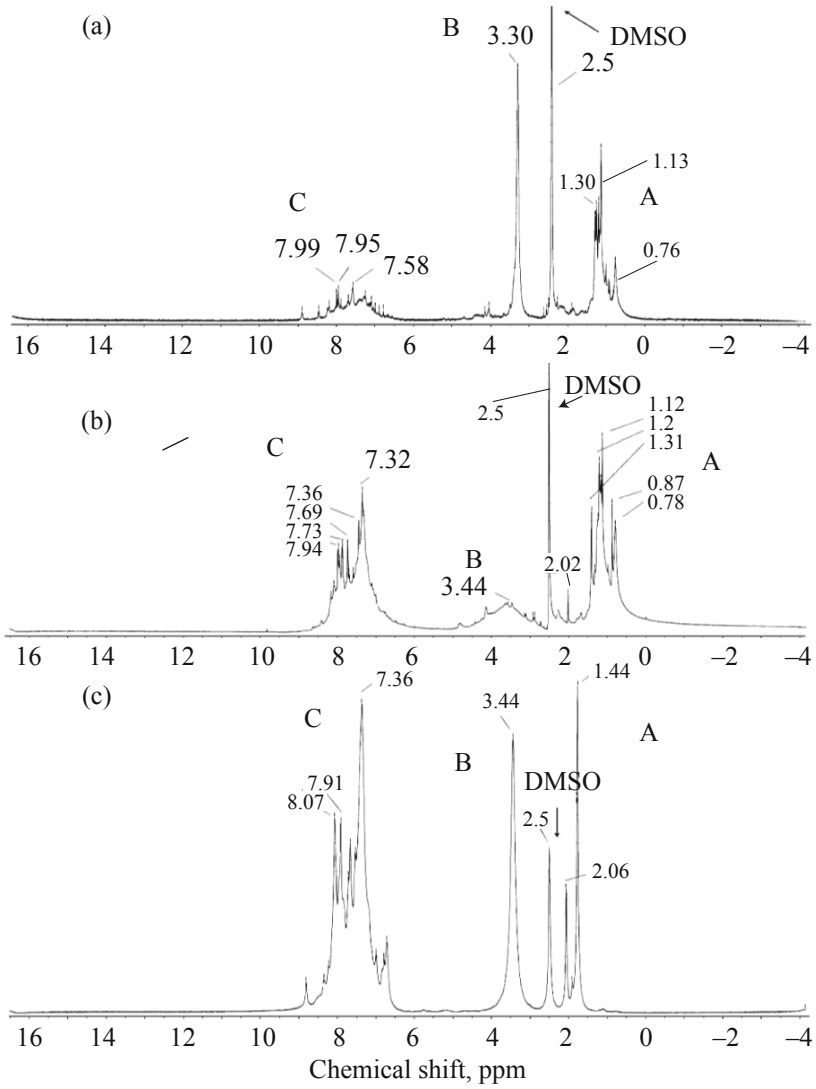

Fig. 12. [1]H NMR spectra of the polymer samples in three different solvents: (a) *n*-decane, (b) THF and (c) acetonitrile.

the solvent that are attached to the polymer, or moving of the main polymer chains. In addition, for some polymers, T_g can be below 25°C or it has temperature range in which case the polymer is soft and flexible at 25°C (for example rubbers). In the following, the two exothermic heat flows, the first peak at 158.5°C and the second peak at 291.8°C observed in the DSC thermogram are shown in Fig. 11. It could be explained by a crystallization phase or transformation of this phase to another structure form followed by branching and/or crosslinking or the high degree of aromaticity with branching and/or crosslinking of the polymer sample [51–53]. The second peak was due to an endothermic reaction at 192.5°C which is related to T_m of the polymer sample. Due to the thermal results obtained from the polymer sample, it can be confirmed that it is sticky and branched polymer with side groups including solvent, connected to the main chain, including solvent.

Structural analysis. The structure of the polymer sample including the type of the functional groups and the chemical structure as well as elemental analysis of the polymer structure were also studied. For this purpose, FTIR, [1]H NMR, [13]C NMR spectroscopies and elementary analysis have been investigated separately on the polymer sample. Initially, the effect of solvent in the polymerization process was investigated. In addition to the primary solvent (*n*-decane), two other solvents (THF and acetonitrile) were also used in the polymer synthesis, in accordance with the steps in the preparation of polymers in experimental section. After the preparation of three types polymers with three different solvents (a: *n*-decane, b: THF and c: acetonitrile) according to the

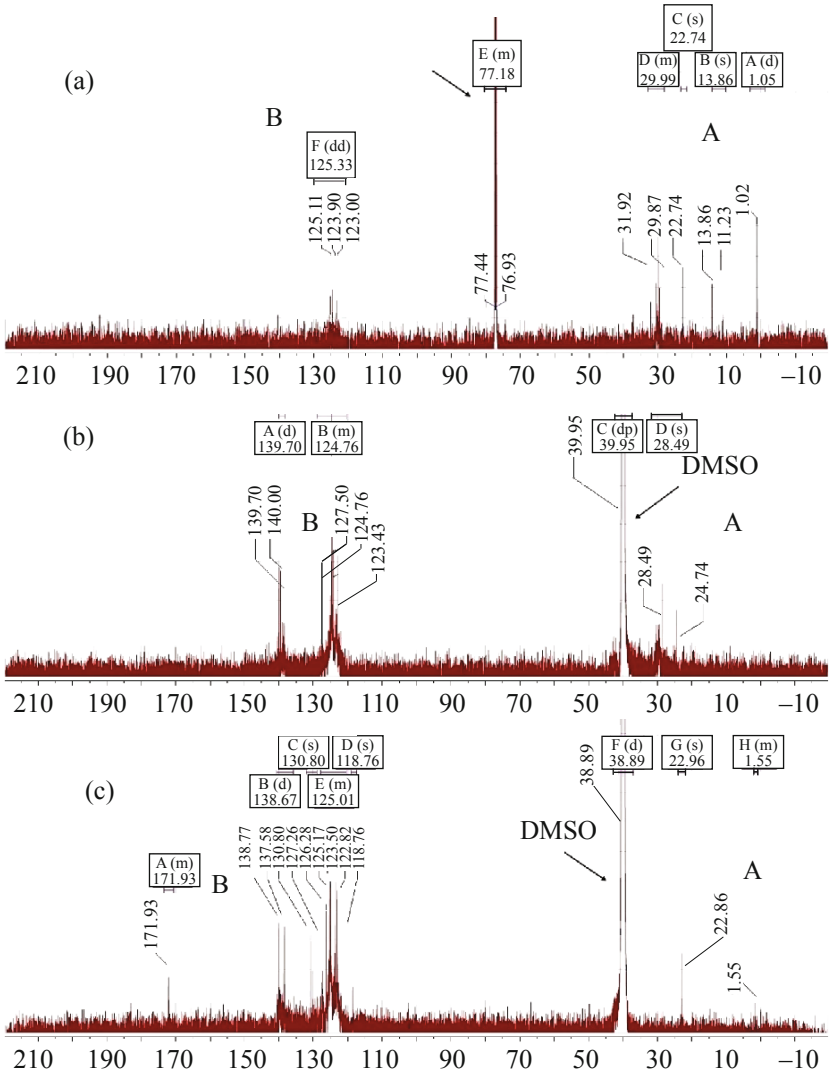

Fig. 13. (Color online) ^{13}C NMR spectra of the polymer samples in three different solvents: (a) *n*-decane, (b) THF and (c) acetonitrile.

procedure expressed in the experimental section, the structure of the synthesized samples was detected by two types of analyses. Based on the structure of the polymer suggested by Neumann [36], the presence of aromatic and aliphatic groups was investigated by ^{1}H and ^{13}C NMR spectroscopy afterward, by using FTIR spectra, the types of functional groups were assigned.

^{1}H NMR and ^{13}C NMR spectroscopy. The ^{1}H NMR spectra (300 MHz) of the representative samples in three different solvents are shown in Fig. 12. There are three graphs in this diagram that Fig. 12a relating to the polymer prepared in *n*-decane, Fig. 12b in THF and Fig. 12c in acetonitrile. In ^{1}HNMR spectrum of Fig. 12, three distinct regions are appeared, a region with peaks at 0.76–1.3 ppm (A in Fig. 12a), 0.78–1.31 ppm (A in Fig. 12b), 1.77–2.06 ppm (A in Fig. 12c), a region with a peak at 3.30 ppm (B in Fig. 12a), and at 3.4 ppm in two regions B in Fig. 12b and Fig. 12c and also a broad set of resonances at 7.0–9.0 ppm (A, B, and C in Figs. 12a–12c). The resonances in region A was demonstrated $–CH_2$ and $–CH_3$ and also $–CH_2$ groups was detected at 3.3–3.4 ppm (B). Aromatic groups include sulfur and without sulfur is shown in region C at 7.3–7.6 ppm [54–58]. By observing the peaks development in all three graphs of Fig. 12, it is seen that the solvent completely affects the polymerization process and the chemical structure of the polymer composition, as in Fig. 12a, the effect of the aliphatic groups is completely evident. This trend in the second and third graphs were less and less. It can be explained by intermolecular forces and chemical structure solvents.

In addition, ^{13}C NMR has been provided to determine the structure details of the polymer samples. In Fig. 13,

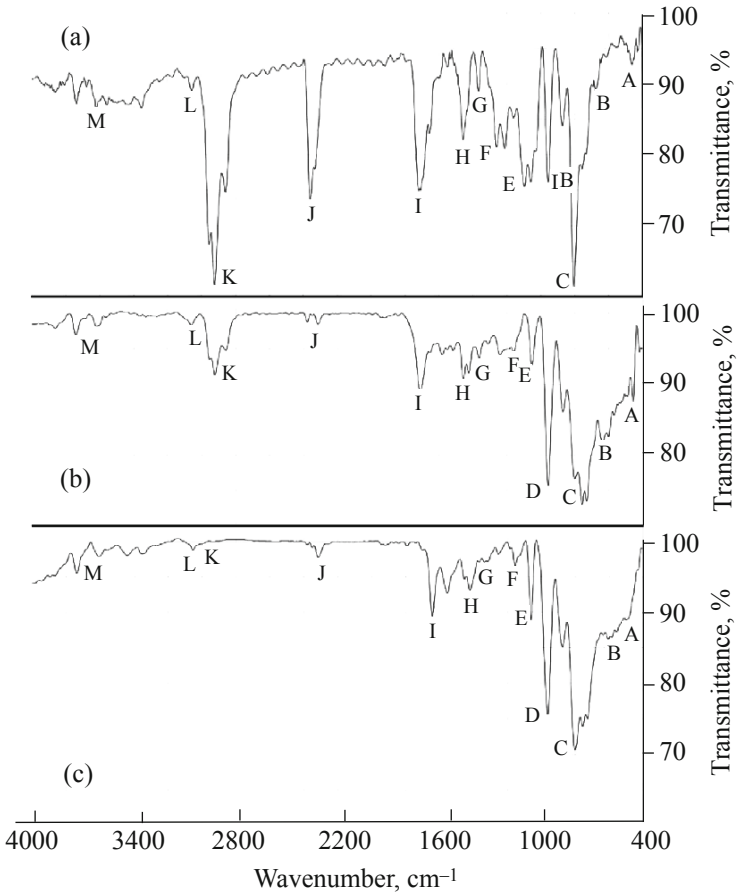

Fig. 14. FTIR spectra of the polymer samples in three different solvents: (a) *n*-decane, (b) THF and (c) acetonitrile.

as same as in Fig. 12, the classification of the graphs is based on the solvents used in the polymer synthesis. The graphs in Fig. 13 are ^{13}C NMR spectra of the polymer samples in *n*-decane (Fig. 13a), in THF (Fig. 13b), and in acetonitrile (Fig. 13c). In each instance, the resonances below 40 ppm (A) are assigned to the methyl carbons (aliphatic groups) in the repeating unit, and the number of resonances depends on the different solvents structures used. The resonances in the rage of 110–160 ppm (B) are assigned to the aromatic carbons in the polymer structure [59]. Interestingly, decreasing peak of the aliphatic groups and increasing peak of aromatic groups in the prepared polymer structure was observed from *n*-decane to acetonitrile.

FTIR spectra. To support the results of ^{1}H and ^{13}C NMR spectroscopy analyses, FTIR spectra were also provided. Peak areas are also shown by English capital letters. As can be seen from Fig. 14, the IR spectra of the polymer samples as follows: A: C–S–S–C dihedral bend (dimethyl disulfide) (450–500 cm^{-1}), B: C–S and few thiophene dications (600–750 cm^{-1}), C and D: (aromatic group $=CH_2$ and C=C and few thiophene dications) (790–980 cm^{-1}), E and F: (C–C and C=S) (1050–1240 cm^{-1}), G and H: (the thiophene symmetrical C=C) (1370–1470 cm^{-1}), I: (aromatic group C=C and phenyl group) (1620–1700 cm^{-1}), J: (S–H (thiol)) (2350–2500 cm^{-1}), K: aliphatic (alkanes) ($–CH_2–$ and $–CH_3$ branching on the benzene ring) (2900–3000 cm^{-1}), L: (aromatic $=CH_2$ and =C–H) (3050–3100 cm^{-1}), M: (O–H group) (3400–3700 cm^{-1}) [60, 61]. However, in this figure, there is a decreasing and increasing trend in aliphatic and aromatic groups. For example, E, F and K points on Fig. 14a has the highest value and in Fig. 14c the lowest value. This indicates the intensity of the aliphatic group in various polymeric samples with different solvents. Also, stretch intensity the point of D can be seen equal in all three diagrams (Figs. 14a–14c). This is due to the formation of the same number of polymer base (polymer monomer) in all three types of samples, which is a repeatable thiophene groups in the polymer structure

Table 3 The results of elementary analysis

Prepared polymers	Elementary analysis, %			
	C	H	S	N
Sample 1 (solvent: *n*-decane)	57.7	5.2	9.7	–
Sample 2 (solvent: THF)	49.4	4.58	12.5	–
Sample 3 (solvent: acetonitrile)	37.1	2.99	14.1	–

and/or it can be deduced that the polymer chains is formed from the thiophenic ring [60, 61]. Another important point that is completely evident, the decrease in the intensity of the thiol group from Fig. 14a to Fig. 14c. Which can indicate the banding of aliphatic groups such as methyl to sulfur, which is evident at the point A of the Fig. 14a then Figs. 14b and 14c.

Elemental analysis. Elemental analysis was used to inspect the role of the reaction solvent on the polymerization process. As shown in Table 3, the percentage of the carbon reduction can be seen from sample 1 to sample 3. This could be another reason for the presence of solvent in the polymerization reaction. On the other hand, the smallest amount in the third sample indicates the strong intermolecular force of the acetonitrile in comparison with other solvents which did not has the tendency to participate in the polymerization reaction. Additionally, this lack of interest in the polymerization reaction can be observed in the absence of nitrogen in sample 3.

CONCLUSIONS

The purpose of this study was to identify and investigate desulfurization of BT in *n*-decane as a model fuel using SiO_2-supported polyoxometalate catalyst with Keggin structure. In addition, the products of the OPD process were fully characterized. As sulfur dioxide from the liquid fuel after the process was about 81% and the solid product formed by polymer evaluations. GPC analysis revealed two important points about the polymer. First, this material separated from the catalyst was a polymer because it had a weighted average molecular weight (M_w) of 183030 Da. Second, the polymer was most likely a branched species so that the monomer concentration had an important role in reducing the polymerization time and formation of high molecular weight polymer. Thermal analysis results of the polymer showed that it could be considered as a crosslinked and sticky, branched with a network structure. The structural analysis such as NMR and FTIR spectroscopies and elemental analysis also indicated the polymer structure type, functional groups, and solvent effect on the polymer structure. The solvents with weaker intermolecular force could participate in the polymerization process and affect the polymer structure. On the other hand, a solvent with stronger intermolecular force such as acetonitrile was ineffective on the polymerization process and did not affect the polymer structure.

CONFLICT OF INTEREST

The authors state that they have no conflict of interest to be disclosed in the present communication.

REFERENCES

1. Bazyari, A., Khodadadi, A.A., Mamaghani, A.H., Beheshtian, J., Thompson, L.T., & Mortazavi, Y., *Appl. Cat.B: Env.*, 2016, vol. 180, pp. 65–77.
2. Raj, J.J., Magaret, S., Pranesh, M., Lethesh, K.C., Devi, W.C., and Mutalib, M.A., *Sep. & Pur. Tech.*, 2018, vol. 196, pp. 115–123.
3. Zhu, W., Huang, W., Li, H., Zhang, M., Jiang, W., Chen, G., and Han, C., *Fuel Process. Tech.*, 2011, vol. 92, no. 10, pp. 1842–1848.
4. Mandizadeh, S., Salavati-Niasari, M., and Sadri, M., *Sep. & Pur. Tech.*, 2017, vol. 175, pp. 399–405.
5. Budukva, S., Klimov, O., Pereyma, V.Y., and Noskov, A., *Russian J. Appl. Chem.*, 2017, vol. 90, no. 9, pp. 1425–1432.
6. Choi, A.E.S., Roces, S., Dugos, N., and Wan, M.-W., *Sustainable Env. Res.*, 2016, vol. 26, no. 4, pp. 184–190.
7. Wang, G., Han, Y., Wang, F., Chu, Y., and Chen, X., *Reaction Kinetics, Mechanisms & Catalysis*, 2015, vol. 115, no. 2, pp. 679–690.
8. Rezvani, M.A., Khandan, S., and Sabahi, N., *Energy & Fuels*, 2017, vol. 31, no. 5, pp. 5472–5481.
9. Zheng, H., Sun, Z., Chen, X., Zhao, Q., Wang, X., and Jiang, Z., *Appl. Catalysis A: General*, 2013, vol. 467, pp. 26–32.
10. Bazyari, A., Mortazavi, Y., Khodadadi, A.A., Thompson, L.T., Tafreshi, R., Zaker, A., and Ajenifujah, O.T., *Appl. Catalysis B: Env.*, 2016, vol. 180, pp. 312–323.
11. Khodaei, B., Sobati, M.A., and Shahhosseini, S., *Clean Tech. & Env. Policy*, 2016, vol. 18, no. 8, pp. 2677–2689.

12. Song, H., Zhu, N., Chen, B., Wang, F., Bai, M., and Wang, X., *Russ. J. Appl. Chem*, 2016, vol. 89, no. 12, pp. 2076–2083.
13. Karami, E., Sobati, M.A., Khodaei, B., and Abdi, K., *Appl. Thermal Eng.*, 2017, vol. 118, pp. 691–702.
14. Rezvani, M.A., Shaterian, M., Akbarzadeh, F., and Khandan, S., *Chem. Eng. J.*, 2018, vol. 333, pp. 537–544.
15. Rahimi, M., Shahhosseini, S., and Movahedirad, S., *Ultrasonics Sonochem.*, 2017, vol. 39, pp. 611–622.
16. Jing Zhang, J., Yi Wang, W., Jian Wang, G., Song, H., and Wang, L., *Russ. J. Appl. Chem.*, 2018, vol. 91, no. 9, pp. 1513–1519.
17. Akbari, A., Omidkhah, M., and Darian, J.T., *Ultrasonics Sonochem.*, 2015, vol. 23, pp. 231–237.
18. Harutyunyan, R., Rezvani, M., and Heravi, M.M., *Syn. & Reactivity in Inorg., Metal-Org, & Nano-Metal Chem.*, 2011, vol. 41, no. 1, pp. 94–99.
19. Rodikova, Y.A., Zhizhina, E.G., and Pai, Z.P., *Reaction Kinetics, Mechanisms & Catalysis*, 2018, vol. 124, no. 2, pp. 469–485.
20. Huang, P., Liu, A., Kang, L., Dai, B., Zhu, M., and Zhang, J., *Chem. Select*, 2017, vol. 2, no. 14, pp. 4010–4015.
21. Proust, A., Matt, B., Villanneau, R., Guillemot, G., Gouzerh, P., and Izzet, G., *Chem. Soc. Rev.*, 2012, vol. 41, no. 22, pp. 7605–7622.
22. Genovese, M. and Lian, K., *Current Opinion in Solid State & Materials Sci.*, 2015, vol. 19, no. 2, pp. 126–137.
23. Wang, S.-S. and Yang, G.-Y., *Chem. Rev.*, 2015, vol. 115, no. 11, pp. 4893–4962.
24. Zhang, Y., Zhang, D., Zhang, J., Zhang, Y., Liu, L., Zhang, X., Feng, Y., Sha, J., Zhang, Y., and Wang, C., *Inorg. Chem. Comm.*, 2016, vol. 74, pp. 6–11.
25. Maerten, S.G., Voß, D., Liauw, M.A., and Albert, J., *Chem. Select*, 2017, vol. 2, no. 24, pp. 7296–7302.
26. Cao, J., Xu, C., Liu, C., and Liu, W., *Chem.Select*, 2016, vol. 1, no. 6, pp. 1268–1272.
27. Shojaei, A.F., Rezvani, A.M., and Heravi, M., *J. Serbian Chem. Soc.*, 2011, vol. 76, no. 11, pp. 1513–1522.
28. Rafiee, E., and Eavani, S., *J. Molecular Liq.*, 2014, vol. 199, pp. 96–101.
29. Mizuno, N., Kamata, K., and Yamaguchi, K., *Bifunctional Molecular Catalysis*, Springer, 2011, pp. 127–160.
30. Zhu, W., Wu, P., Chao, Y., Li, H., Zou, F., Xun, S., Zhu, F., and Zhao, Z., *Industrial & Eng. Chem. Res.*, 2013, vol. 52, no. 49, pp. 17399–17406.
31. Mizuno, N. and Kamata, K., *Coordination Chem. Rev.*, 2011, vol. 255, no. 19–20, pp. 2358–2370.
32. Xiao, J., Wu, L., Wu, Y., Liu, B., Dai, L., Li, Z., Xia, Q., and Xi, H., *Appl. Energy*, 2014, vol. 113, pp. 78–85.
33. Li, J., Hu, B., Tan, J., and Zhuang, J., *Transition Metal Chem.*, 2013, vol. 38, no. 5, pp. 495–501.
34. Yan, X.-M., Mei, P., Xiong, L., Gao, L., Yang, Q., and Gong, L., *Catalysis Sci. & Technology*, 2013, vol. 3, no. 8, pp. 1985–1992.
35. Choi, A.E.S., Roces, S., Dugos, N., and Wan, M.-W., *Fuel*, 2016, vol. 180, pp. 127–136.
36. Khenkin, A.M. and Neumann, R., *ChemSusChem*, 2011, vol. 4, no. 3, pp. 346–348.
37. Mothé-Esteves, P., Pereira, M.M., Arichi, J., and Louis, B., *Crystal Growth & Design*, 2010, vol. 10, no. 1, pp. 371–378.
38. Arichi, J., Pereira, M.M., Esteves, P.M., and Louis, B., *Solid State Sci.*, 2010, vol. 12, no. 11, pp. 1866–1869.
39. Tsigdinos, G.A. and Hallada, C.J., *Inorg. Chem.*, 1968, vol. 7, no. 3, pp. 437–441.
40. Khenkin, A.M., Weiner, L., Wang, Y., and Neumann, R., *J. Am. Chem. Soc.*, 2001, vol. 123, no. 35, pp. 8531–8542.
41. Neumann, R. and Lissel, M., *J. Org. Chem.*, 1989, vol. 54, no. 19, pp. 4607–4610.
42. Khenkin, A.M., Leitus, G., and Neumann, R., *J. Am. Chem. Soc.*, 2010, vol. 132, no. 33, pp. 11446–11448.
43. Domb, A.J. and Langer, R., *J. Polymer Sci. Part A: Polymer Chem.*, 1987, vol. 25, no. 12, pp. 3373–3386.
44. Zohuriaan, M.J. and Shokrolahi, F., *Polymer Testing*, 2004, vol. 23, no. 5, pp. 575–579.
45. Shortt, D.W., *J. Liq. Chrom.*, 1993, vol. 16, no. 16, pp. 3371–3391.
46. Atkins, P. and de Paula, J., *Phys. Chem. Life Sci.*, OUP Oxford, 2011.
47. Wong, A.C.Y. and Lam, F., *Polymer Testing*, 2002, vol. 21, no. 6, pp. 691–696.
48. Sperling, L.H., *Introduction to Physical Polymer Sci.*, Wiley, 2005.
49. Stutz, H., Illers, K.-H., and Mertes, J., *J. Polymer Sci. Part B: Polymer Physics*, 1990, vol. 28, no. 9, pp. 1483–1498.
50. Nielsen, L.E., *J. Macromol. Sci., Part C*, 1969, vol. 3, no. 1, pp. 69–103.
51. Kimura, H., Matsumoto, A., Sugito, H., Hasegawa, K., Ohtsuka, K., and Fukuda, A., *J. Appl. Polymer Sci.*, 2001, vol. 79, no. 3, pp. 555–565.

52. Akkara, J.A., Senecal, K.J., and Kaplan, D.L., *J. Polymer Sci. Part A: Polymer Chem.*, 1991, vol. 29, no. 11, pp. 1561–1574.
53. Maleki, A., Aghaei, M., Hafizi-Atabak, H.R., and Ferdowsi, M., *Ultrasonics Sonochemistry*, 2017, vol. 37, pp. 260–266.
54. Zhang, Z., and Feng, S.-S., *Biomaterials*, 2006, vol. 27, no. 2, pp. 262–270.
55. Guo, T., Yu, L., Zhao, B., Ying, L., Wu, H., Yang, W., and Cao, Y., *J. Polymer Sci. Part A: Polymer Chem.*, 2015, vol. 53, no. 8, pp. 1043–1051.
56. Son, S.-K., Choi, Y.-S., Lee, W.-H., Hong, Y., Kim, J.-R., Shin, W.-S., Moon, S.-J., Hwang, D.-H., and Kang, I.-N., *J. Polymer Sci. Part A: Polymer Chem.*, 2010, vol. 48, no. 3, pp. 635–646.
57. Kim, E., Choi, Y.-K.and Lee, M.-H., *Macromolecules*, 1999, vol. 32, no. 15, pp. 4855–4860.
58. Chen, C.-P., Chan, S.-H., Chao, T.-C., Ting, C.and Ko, B.-T., *J. Am. Chem. Soc.*, 2008, vol. 130, no. 38, pp. 12828–12833.
59. Wang, Y.-X. and Ishida, H., *Macromolecules*, 2000, vol. 33, no. 8, pp. 2839–2847.
60. Pavia, D.L., Lampman, G.M., Kriz, G.S., and Vyvyan, J.A., *Introduction to Spectroscopy*, Cengage Learning, 2008.
61. Heyes, D.M. and Okumura, H., *J. Chem. Physics*, 2006, vol. 124, no. 16, pp. 164501.